Chapter 4

DEBRIS MOVEMENT AT IEG

4.1. INTRODUCTION

In the μED-milling process, the occurrence of spark at the random position in the IEG results in the discharge craters being uniformly distributed on the workpiece. This results in good surface finish, but repeated sparking at the same location may deteriorate the surface finish. The molten metal ejected from the workpiece flows in the form of globules [86]. When the quantity of the ejected metal is less, then stirring action caused by tool rotation breaks the globules into small particles [87]. These particles on cooling due to dielectric fluid generates spherical particles or debris. The size of debris varies from 1 nm to about 50 μm [88]. The volume of crater removed from the workpiece is approximately equal to the measured amount of debris [89]. The shape of the crater formed on the workpiece depends on the type of dielectric used such as air or liquid [90]. The debris are continuously formed during the machining process and it will cause major problems in the μED-milling as these are electrically conductive. Its presence at one location in large number gives rise to secondary discharge causing a disturbance in sparking, and its movement may affect the geometry of μchannel due to redeposition.

Effective flushing of debris from the gap improves the performance of μED-milling process. The necessary drive for debris movement along the gap is provided by tool rotation speed. The movement of debris, its trajectory, and position are important factors to study the accretion (accumulation) of debris on the workpiece surface. The tool rotation changes the fluid flow pattern in the gap, and the debris will follow the fluid pattern. The vortex flow created due to tool rotation in the channel increases the concentration of debris in that region [91]. Discrete phase modeling (DPM) in Fluent is used to study the movement of debris in the gap and to understand the fluid debris interaction and subsequent redeposition. The details of DPM is discussed in chapter 2 under section 2.4.

4.2. OBSERVATION POINTS

The debris movement in the gap is analyzed using the model used for dielectric fluid study and the observation points selected are schematically represented in Figure 4.1. The analysis is carried out by considering certain references along the IEG and across IEG. In Figure 4.1, three different sections along IEG are considered for particle injection and the sections are represented as center section (CS), top section (TS), and bottom section (BS). The CS is parallel to horizontal axis whereas TS and BS are at an angle of 45° on either side of CS. Even though in the actual process the particles are continuously formed along the sparking area, but for simulation, only three sections are considered which is expected to reasonably capture the actual behavior of the process. The section across IEG is divided equally and are named as A, B, and C. The position A represents near the tool, position B at the center, and position C near the workpiece. The particle injected from the workpiece surface will reach any of these three positions depending on injection velocity.

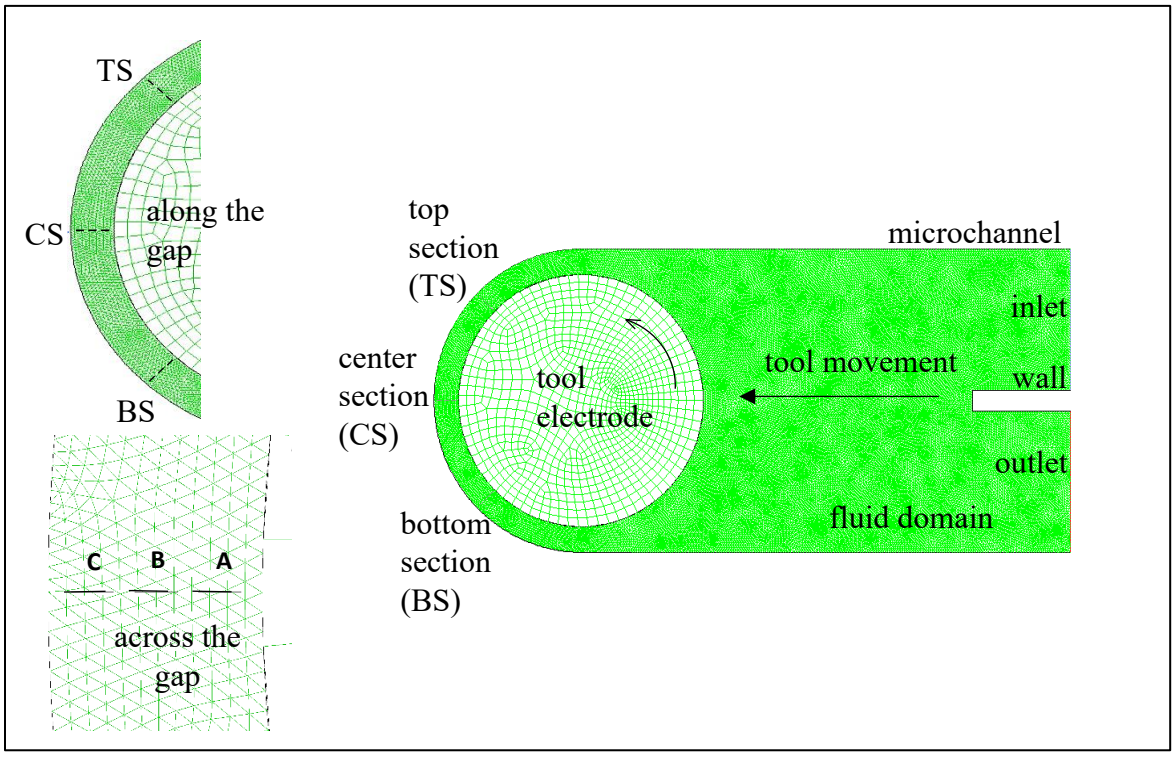

Figure 4.1 Schematic diagram showing the analysis points for studying motion of debris

4.3 BOUNDARY CONDITIONS

The particles can exchange mass, momentum and energy with the dielectric fluid. Four different boundary conditions of the surface used in DPM study is represented in Figure 4.2 and the DPM parameters used for simulation is listed in Table 4.1. These boundary conditions are reflect, trap, escape and wall jet. When the particle hits the surface with reflect boundary condition, it rebounds from the surface with a change in its momentum and direction. In case of trap and escape boundary condition, trajectory calculations are terminated when the particle touches the surface and the number of particles trapped or escaped from the boundary is calculated. The wall jet boundary condition is used for high-temperature walls where the spray acts as a jet. For simulation, inlet and outlet of the model are given with escape boundary condition and particle injection surface is given with wall jet boundary condition. All other surfaces are given as reflect boundary condition. The spherical-shaped steel particles of size 4, 8, and 12 μm are injected from the workpiece surface with a flow rate of 0.001 g/s. Unsteady particle tracking with spherical drag law is used to track the particles in the fluid domain. The simulation uses surface type injection of particles which is similar to the process happening in the μED-milling process. The erosion/accretion physical model is used to calculate the accretion of a particle on the workpiece and tool surface. No slip boundary condition is applied to the workpiece surface. The effect of spark, electrostatic force acting on the tool and gravity effect is neglected. The accretion (accumulation) rate of particles are calculated at wall boundaries. The accretion rate is calculated in units of material addition/(area-time), i.e., mass flux (g/mm^2 s). The accretion rate is given as

$$R_{accretion} = \sum_{p=1}^{N_{particles}} \frac{\dot{m}}{A_{face}} \tag{4.1}$$

where A_{face} is the area of the cell face at the wall (mm^2) and $\dot{m}$ is the mass flow rate of particles (g/s) [92].

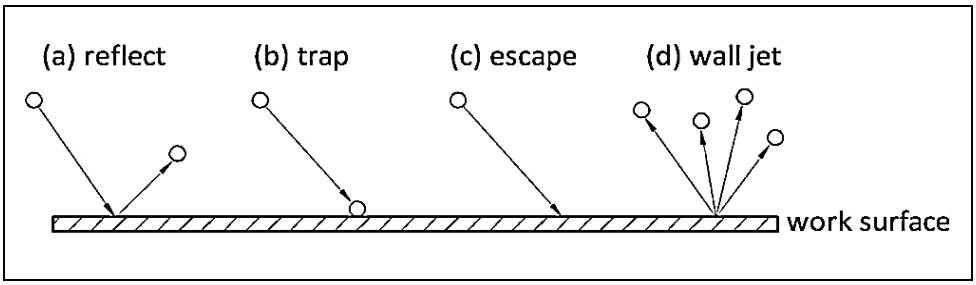

Figure 4.2 Types of boundary conditions for Discrete phase modeling

Table 4.1 DPM parameters

Simulation type	Transient state calculations
Particle treatment	Unsteady particle tracking
Drag law	Spherical
Physical models	Erosion/Accretion
Injection type	Surface
Particle type	Inert, uniform diameter distribution
Diameter / material	4, 8, 12 μm solid steel spherical particles (density = 8.03 g/cm^3, mass = 7.29×10^{-9} g, flow rate = 0.001 g/s)
Inlet	Escape
Outlet	Escape
Wall	Reflect
Injection surface	Wall jet

4.4. BEHAVIOR OF DEBRIS PARTICLES IN IEG

4.4.1. Effect of injection velocity on particle position

The particles are injected with a high velocity from the workpiece surface to reach certain position in the IEG as represented in Figure 4.3. Due to this injection velocity, particle penetrates the moving fluid and reaches a certain position in the gap. When the particle injection velocity is less, it does not travel long distance and remains attached with the workpiece as given in Figure 4.3 (i). On the contrary, when the velocity is very high it

hits the surface of the tool on the opposite side of the workpiece surface as shown in Figure 4.3 (ii). The particles are injected with intermediate velocity of 240, 190 and 125 cm/s to travel 40, 25 and 10 µm distance in the gap to reach the positions A, B, and C respectively as given in Figure 4.3 (iii) to (v). Due to rotation of the tool, particles are dragged from that position and moves along the fluid in the gap.

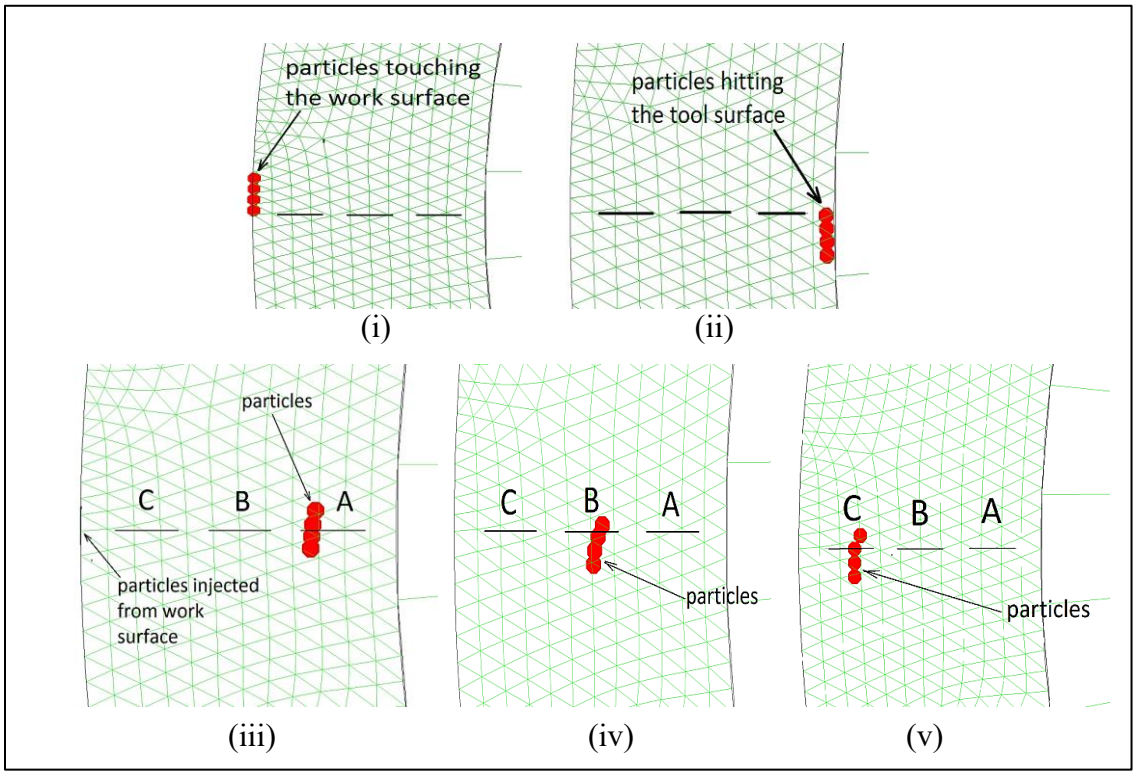

Figure 4.3 Effect of particle injection velocity on the position of particle across the IEG injected normal to the workpiece surface. Particle position in the gap (i) touching the workpiece surface (ii) touching the tool surface (iii) A (near to tool) (iv) B (mid position) (v) C (near workpiece)

4.4.2. Pattern of particle movement

The movement of debris particles in the gap depends upon tool rotation, dielectric flow, and the initial particle velocity. The direction of movement of the debris particles in the gap decides whether the particle accretes on a workpiece surface or gets flushed away by the dielectric. In the simulation, particles are injected from various positions along IEG

and the movement of the particles are tracked. It is observed that particles move along the periphery of the tool due to rotation of the tool and accrete on the workpiece surface. Some particles get accreted on the workpiece surface and some particles get flushed away. During movement of a particle along the periphery of the tool, the chain-like structure is formed. In die-sink EDM, the chain-like bridge is formed normal to the electrode surface [91], but in the μED-milling, it is observed that chain-like structure is formed along the periphery of the tool and along the vortex at the back of the tool. These particles which moved away from the gap come across the vortex at the back of the tool.

The particles that are trapped in the vortex follow a rotary path and experience a centrifugal force. It also experiences a drag force that causes the particle to move towards the center of the vortex. When both the force is balanced, then the particles travel in a circular path. The particles trapped in the vortex is denser than the fluid, and hence the centrifugal force tends to move the particles to the outer edge of the vortex. Moreover, if the particles are lighter than the fluid, then it tends to move the particles towards the center of the vortex which is not visible in the present simulation as the density of particles is higher than the dielectric. The particles collected at the boundary of the vortex get flushed away by the linear motion of the tool as machining proceeds. Different size particles combine to form a cluster of particles in the gap which is observed in Figure 4.4 (a). Hence new schematic representation of particle behavior for the μED-milling process is proposed and represented in Figure 4.4 (b). Common behaviors of particles observed in the gap are (i) accretion on workpiece surface, (ii) cluster of a particle in the gap, and (iii) chain-like structure. The behaviors are similar to results proposed by Furutani et al. [94] on surface modification in die-sink EDM in which he observed four types of particle behavior between the electrodes as depicted in Figure 4.5. These behaviors are named as reciprocating motion, adhesion on electrode, cluster in a gap, and chain of particles connected between the electrodes. Gatto et al. [95- 96] observed similar results of bridges of debris in the gap in the form of chains and clusters in electrodischarge drilling (EDD) and EDM process as shown in Figure 4.6. The present results of the μED milling process is well correlated with

previous findings of EDM process except for the reciprocating motion of particles which does not happen when tool rotates.

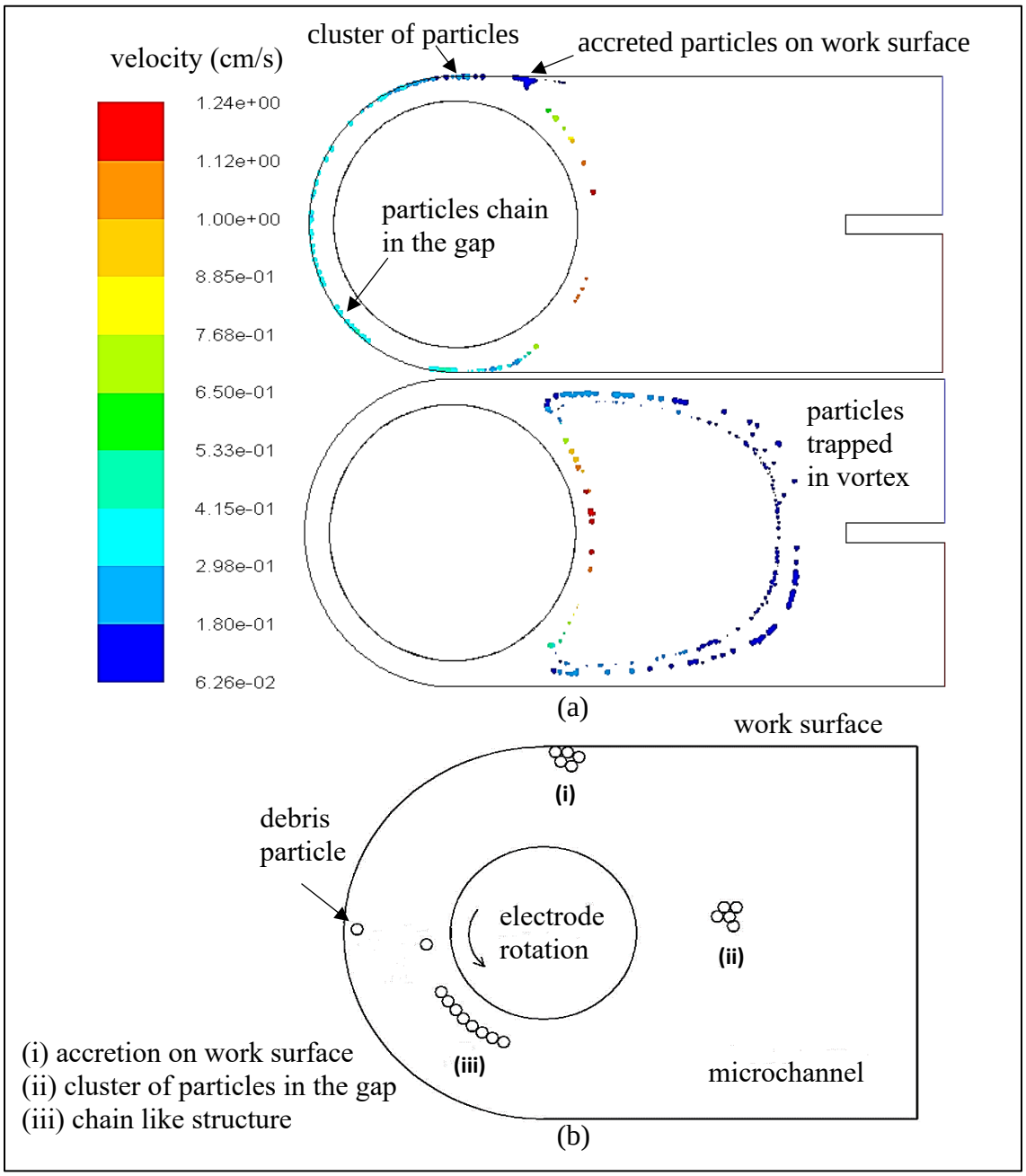

Figure 4.4 (a) Discrete phase modeling showing behavior of particles in the gap and (b) New schematic representation of particle behavior for µED milling process

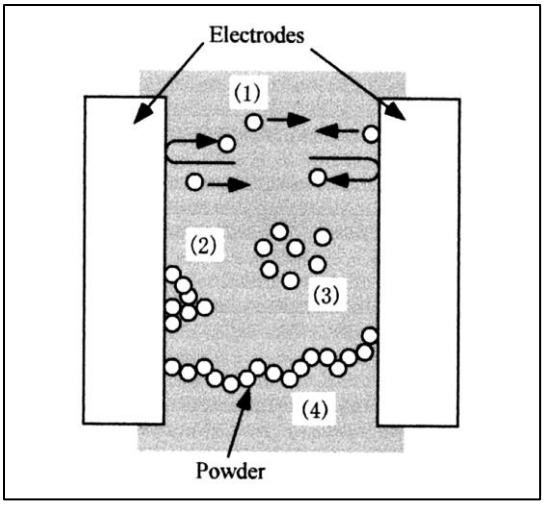

Figure 4.5 Four types of powder behavior in EDM: (1) reciprocating motion, (2) adhesion on electrode, (3) cluster in the gap and (4) chain connecting the electrodes [94]

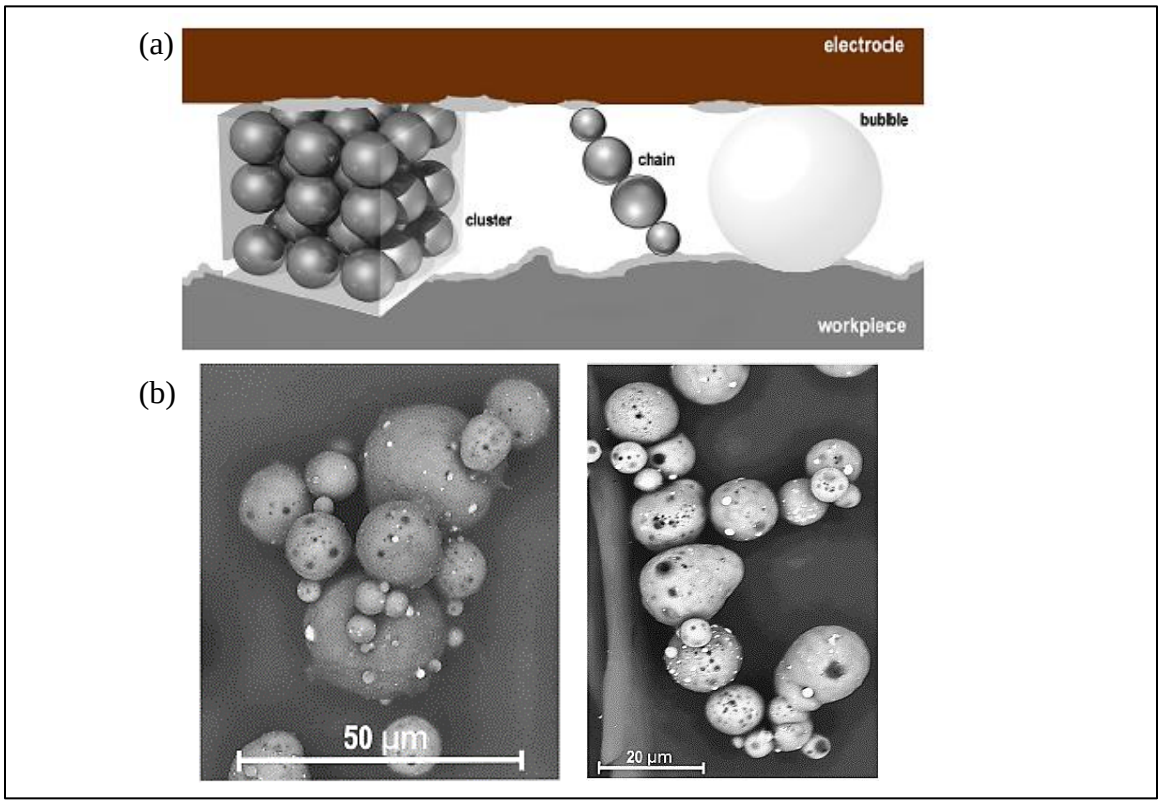

Figure 4.6 (a) Phenomenon occurring during the ignition time: formation of debris clusters, chains, gas bubbles and (b) SEM images of chain and cluster of debris [95-96]

4.4.3. Particle trajectory

In the μED-milling process, as the tool is rotating continuously at high speed, debris particles move along the gap about the periphery of the tool to make multiple rotations before accreting on the workpiece surface. For studying the trajectory, particles are injected from CS at different positions such as A, B, and C in the gap. It is observed that when the particles are injected from position C (near to workpiece), it travels less distance and accretes on the workpiece surface whereas on injection from position A (near to tool), it travels larger distance making multiple rotations around the tool before reaching the workpiece surface. The distance traveled by the particle when injected from position B (mid position) falls between that of position A and position C. The particle trajectories for three different conditions are represented in Figure 4.7. The reason for the large change in trajectory length is attributed to larger dielectric velocity variation across the gap towards the workpiece. The particles near the tool experience larger drag and undergo as many as six rotations before reaching the accretion point. However, particles injected near the workpiece do not recirculate in the gap as these particles are not dragged into the gap due to lower fluid velocity. The agitation of fluid causes swirling of the fluid tangential to the rotation of the tool. The fluid agitating also acts as the driving force between solid particles and fluid. Particle trajectory distance is calculated by recording the location of the particle during iteration until accretion at workpiece surface. These coordinate values of particles are traced in AutoCAD to obtain the distance traveled by the particle. The effect of particle size and tool rotation speed on the distance traveled is presented in Figure 4.8. The particle size of 4, 8, and 12 μm and tool rotation speed of 100, 500, and 800 rpm are considered for simulation. It is observed that at 100 rpm speed, distance traveled by the particle is larger before accreting on the workpiece surface. At lower speed, particle continues to travel and recirculate in the gap making multiple rotations around the tool before accreting on the workpiece surface. At 500 rpm speed, the distance traveled by the particle decreases and this decrease is higher for particles injected from position A (near to tool). The distance traveled by the particle injected from any position of the gap decreases with the increase in tool speed irrespective of the size of the particles. At 800 rpm speed, most of the particles

get flushed away from the gap and get trapped in the vortex at the back of the tool without accreting on the workpiece surface.

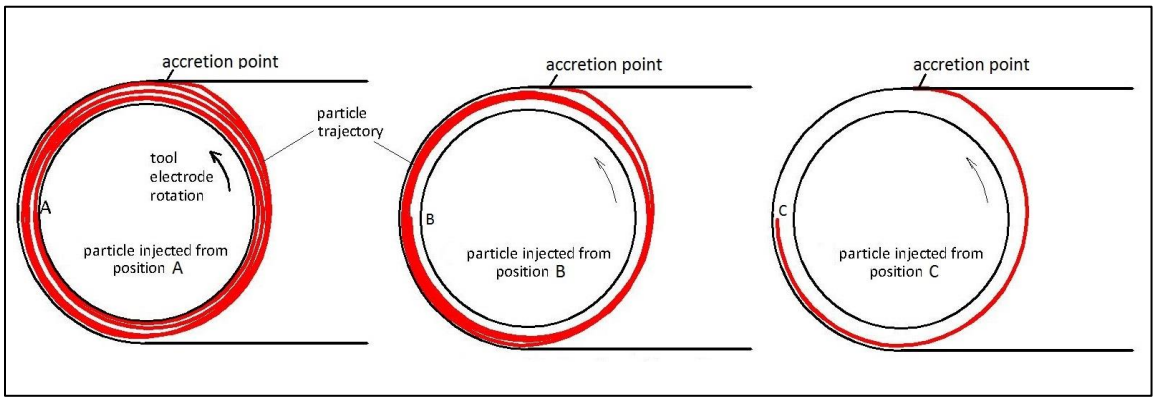

Figure 4.7 Trajectory of debris particles

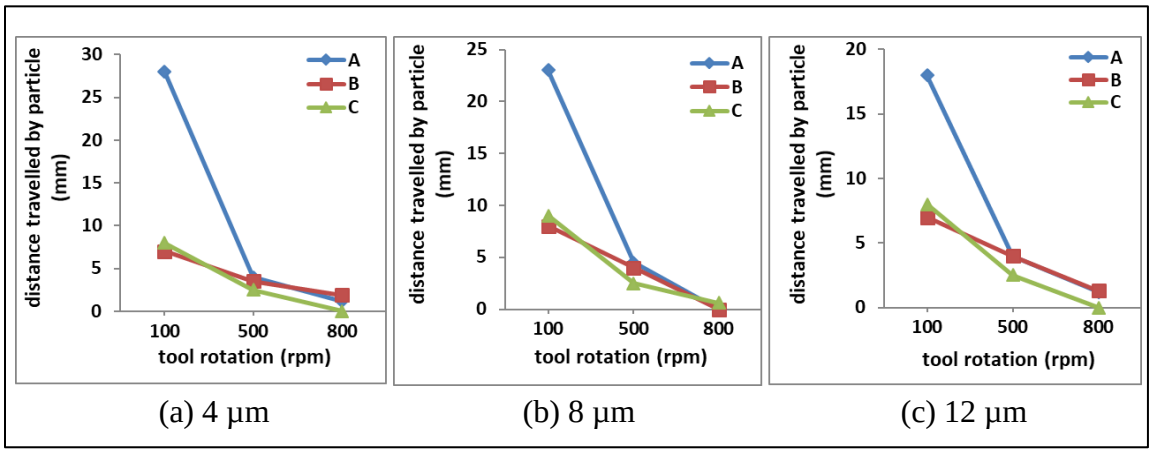

Figure 4.8 Distance travelled by particle (mm) for various electrode speed before accretion for different particle size

4.5. ACCRETION OF DEBRIS PARTICLES

Particles injected from different sections along the gap and from different positions across the gap followed the streamlines of the fluid flow in the gap. After making multiple rotations in the gap, some particles accreted on the workpiece surface and some particles are dragged by the fluid vortex created at the back of the tool. These particles continued to follow the streamlines of the fluid vortex and not accreted on the workpiece surface [97].

It is observed that accretion happens at similar areas on the workpiece surface. For simplification, these areas are classified into two zones: sparking zone and outside the sparking zone as shown in Figure 4.9. Sparking zone is a semi- circular area where the gap size is less and the probability of spark is more. Accretion of particles in the sparking zone increases the deposition layer on the workpiece surface. As a result, repetitive sparks occur in the same area, and the material is removed without affecting the dimension of the μchannel. However, accretion of particles outside the sparking zone increases the deposition layer on the workpiece surface which is not removed from the workpiece surface. This changes the dimension of the μchannel. The results of accretion of the particles injected from different sections (CS, TS, and BS) along the gap and different positions (A, B, and C) across the gap are discussed in detail in the subsequent section.

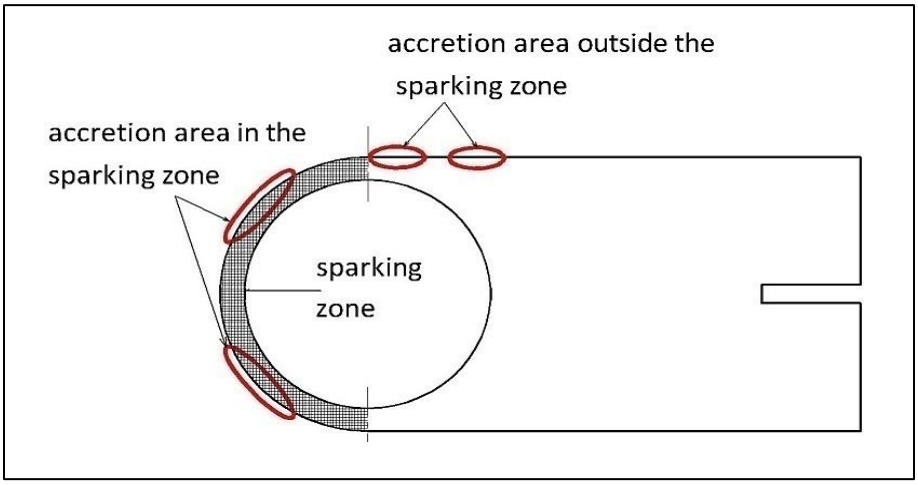

Figure 4.9 Various accretion zone in the μchannel

4.5.1. Particle injection from center section

Spherical size particles are injected from different locations in the gap, and the accretion of particles on the workpiece surface is studied. These injection points represent the position of craters in actual EDM process. However, there can be an infinite number of craters along workpiece surface, and all these points can be the possible source of molten metal and debris. For simulation study, few sections are considered where the probability of crater is more. Simulation results of the particles gave accretion values at various

locations on the workpiece surface. Table 4.2 shows the values of accretion of particles on a workpiece surface when they are injected from CS of the gap for various size and tool rotation speed. The particles lost in the vortex at the back of the tool are not accreted on the workpiece surfaces. The three different cases arise from a position of a particle across the cross section is discussed as follows.

Table 4.2 Accretion of particles ($\times 10^{-4}$ g/mm^2) injected from center section (CS) of gap

Particle size (μm)	Tool speed (rpm)	Position A (near tool)		Position B (at center)		Position C (near workpiece)	
		Inside sparking zone	Outside sparking zone	Inside sparking zone	Outside sparking zone	Inside sparking zone	Outside sparking zone
4	100	-	9	-	28.7	-	16.58
	500	8.61	-	8	-	9.41	-
	800*	-	3.37	0.361	-	-	-
8	100	-	9.25	-	31.2	-	21.7
	500	9.43	-	9	-	9	-
	800*	-	4.7	-	-	-	-
12	100	-	18.3	-	36	-	30.6
	500	9.11	-	9.19	-	9.46	-
	800*	-	8	-	2.26	-	-

*no accretion, loss of particle in recirculation zone

Case I: Particle injection from position A (near to tool)

In this case, it is observed that accretion outside the sparking zone is greater than accretion inside the sparking zone. Total accretion at 100 rpm is greater than total accretion at 800 rpm as there is a loss of particles due to longer travel distance (multiple rotations). With the increase in tool speed, the accretion rate decreases drastically for all positions as given in Figure 4.10. When the diameter of particle increases, the rate of accretion outside the sparking zone found to increase non-linearly. It is observed in both 100 and 800 rpm and hence can be correlated to the size of particles. This result is also observed when the particle is injected from the top and bottom section of the gap as shown in Figure 4.11.

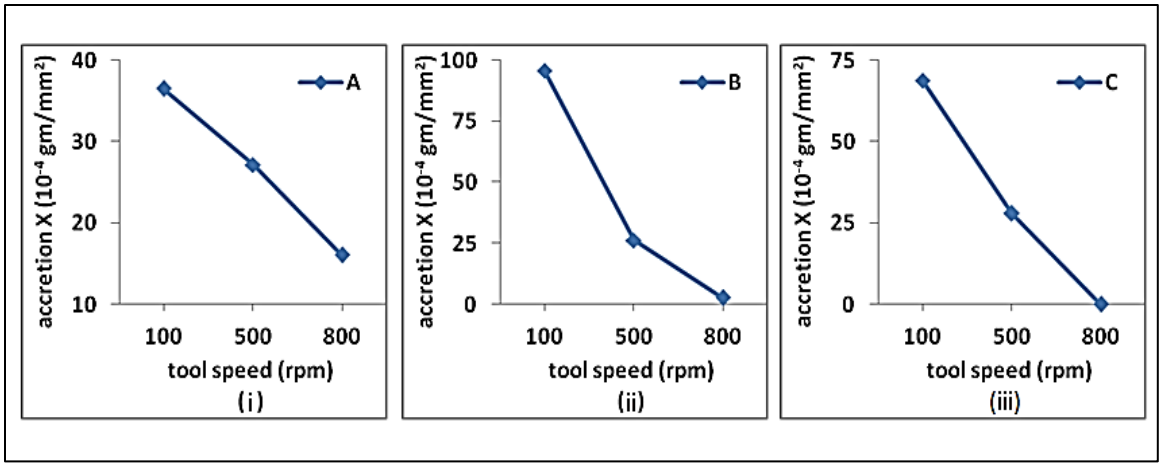

Figure 4.10 Effect of tool speed on total accretion values when all particles are injected from center section (CS) of the gap. Particles injected from position (i) A (near to tool) (ii) B (mid-position) and (iii) C (near to workpiece) of the gap

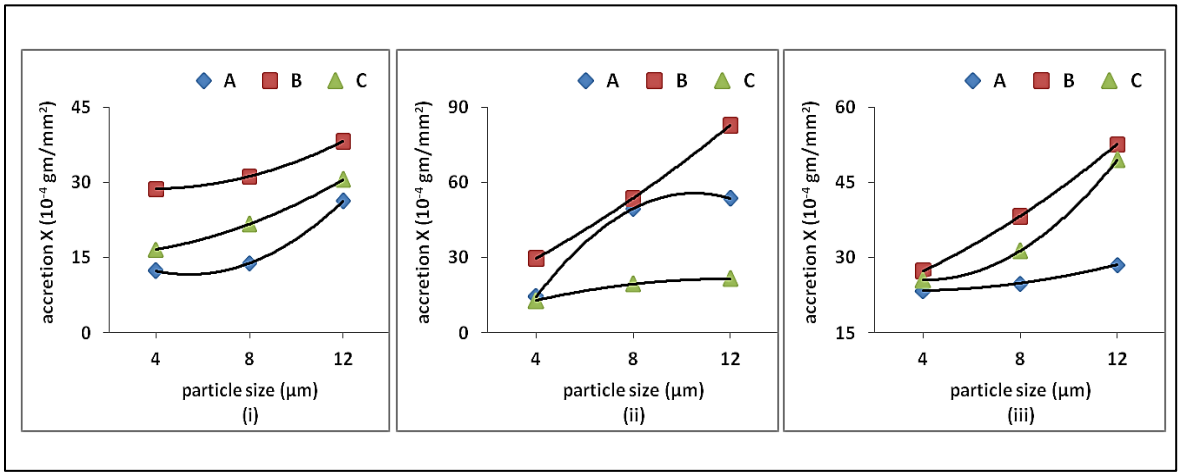

Figure 4.11 Effect of particle size on accretion values outside the sparking zone for all speeds. Particles injected from (i) center section (CS), (ii) top section (TS) and (iii) bottom section (BS) of the gap

Case II: Particle injection from position B (center of the gap)

In this case, it is observed that at 800 rpm, particle undergoes multiple rotations irrelevant of a size which can lead to loss of particle and less accretion outside the sparking zone. At 500 rpm, the accretion almost remains same as the case I and it always happens inside the sparking zone as observed in Figure 4.12 (a) and (b). Hence, 500 rpm is not

going to contribute to change in dimension of μchannel significantly. At 100 rpm, the accretion is found to increase threefold of the case I which can cause to larger accretion at a position outside the sparking zone contributing to change in dimension as observed in Figure 4.12 (c).

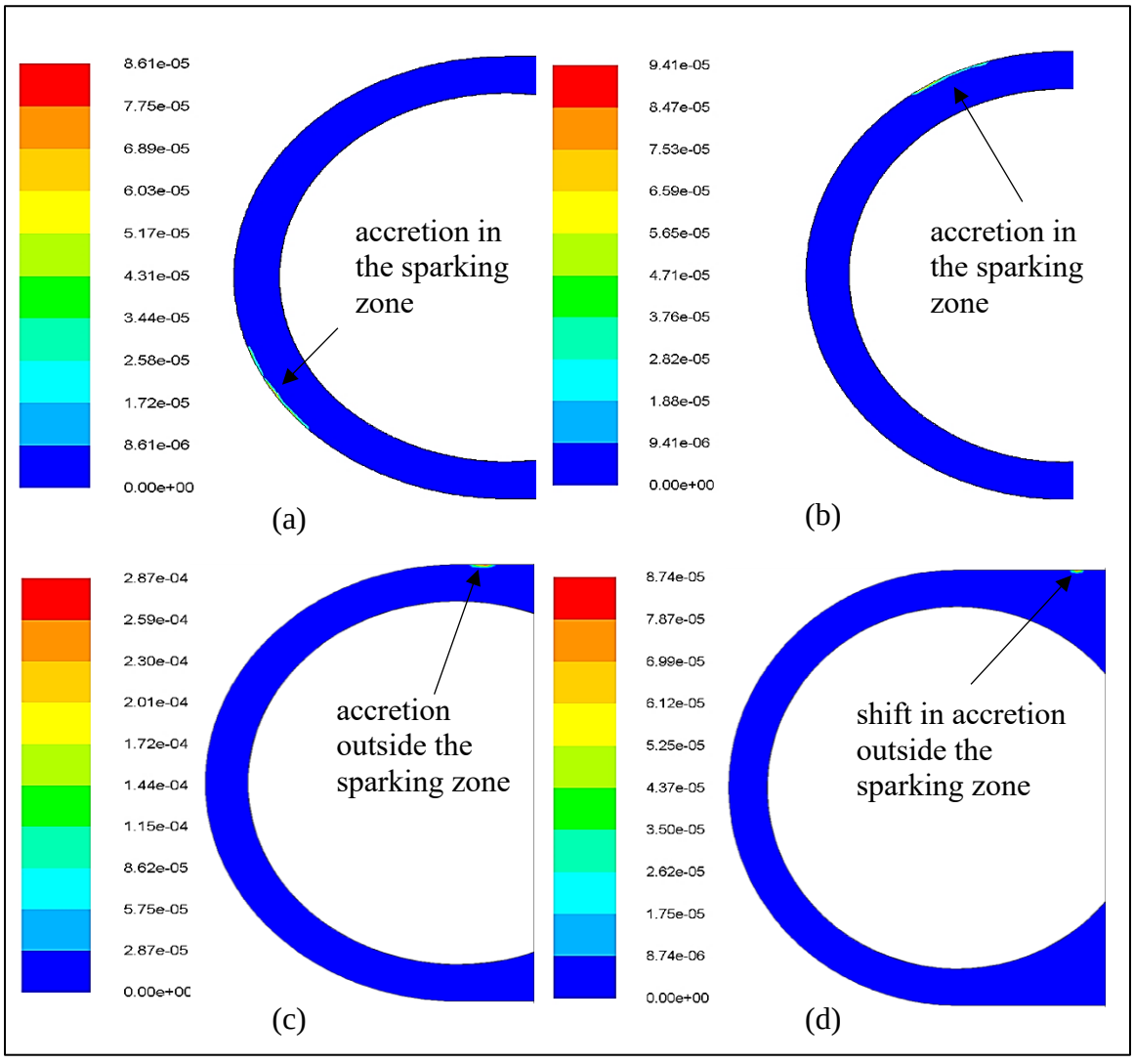

Figure 4.12 Contour plots showing (a), (b) accretion (g/mm^2) in the sparking zone, (c) outside the sparking zone, and (d) shift in accretion outside the sparking zone

Case III: Particle injection from position C (near to workpiece surface)

In this case, it is observed that at 800 rpm, all the particles injected are found to escape the sparking zone without causing any accretion in the sparking zone or outside the sparking zone. This can be considered as an extension of case II where the particle is found to escape the zone due to longer trajectory compared to case I. It continues to remain same at 500 rpm with the similar accretion rate and accretion position. As explained earlier at 100 rpm in case I, due to a greater number of rotations, less accretion happens outside the sparking zone. This is attributed to the loss of particles due to multiple rotations and subsequent escape at the vortex. However, in case II, the number of rotations reduces and accretion rate increases by threefold compared to case I. This clearly indicates the reduction in the travel distance; the loss of particle is also reduced, but the position of accretion remains the same. In case III, there is a shift in the position of accretion in addition to lesser travel distance (half rotation) as shown in Figure 4.12 (d). This shift causes drop in the value of accretion rate compared to case II, but since the trajectory length is smaller, it has larger accretion rate as compared to case I. The accretion inside the sparking zone is removed in subsequent sparking.

4.5.2. Particle injection from top section and bottom section

Particles injected from the top and bottom section of the gap gave similar accretion areas on the workpiece surface with a change in accretion values. The values of accretion for particles injected from the top and the bottom section is listed in Table 4.3 and Table 4.4, respectively. It is observed that accretion happens in the sparking zone when the particle is injected from the position near the tool whereas accretion happens outside the sparking zone when it is injected from the center or near to workpiece. As discussed earlier with the increase in particle size, accretion increases nonlinearly irrespective of the position of injection which is shown in Figure 4.11 (ii) and (iii).

Table 4.3 Accretion of particles ($\times 10^{-4}$ g/mm^2) injected from top section (TS) of gap

Particle size (μm)	Tool speed (rpm)	Position A (near tool)		Position B (at center)	Position C (near workpiece)
		Inside sparking zone	Outside sparking zone	No accretion inside the sparking zone	No accretion inside the sparking zone
				Outside sparking zone	Outside sparking zone
4	100*	-	8.13	5.4	-
	500	-	6.36	11.6	6.75
	800	2.08	-	12.72	6.03
8	100	-	35.01	25.28	5.93
	500	18.3	-	28.5	6.48
	800*	-	14.62	-	7.06
12	100	-	39.06	45.08	15.38
	500	13.9	-	20.06	4.57
	800	-	14.63	17.7	1.68

*no accretion, loss of particle in recirculation zone

Table 4.4 Accretion of particles ($\times 10^{-4}$ g/mm^2) injected from bottom section (BS) of gap

Particle size (μm)	Tool speed (rpm)	Position A (near tool)		Position B (at center)	Position C (near workpiece)
		Inside sparking zone	Outside sparking zone	No accretion inside the sparking zone	No accretion inside the sparking zone
				Outside sparking zone	Outside sparking zone
4	100	-	15.4	18.12	4.32
	500	-	7.98	5.9	5.28
	800	11.01	-	3.37	15.9
8	100*	-	10.09	4.71	-
	500	-	8.43	16.28	18.06
	800	-	6.34	17.29	13.26
12	100	-	6.14	34.4	38.35
	500	-	12.23	10.51	11.18
	800*	-	10.19	7.7	-

4.6. COOLING RATE OF PARTICLES

4.6.1 Analytical Method

The cooling rate of the spherical debris particle is calculated using analytical method and the simulation. In the analytical method, single spherical particle is assumed stationary in the μchannel at a temperature (T = 15000 K). Kerosene flows at a temperature (T_∞ = 300 K) with a certain velocity over a particle. The velocity of the kerosene varies depending upon the position of the particle in the IEG (A, B, C). The diameter of the particle considered are 4, 8, and 12 μm. This can be considered a forced convection heat transfer using the liquid medium. The assumptions made for calculations are steady state operating conditions, radiation heat transfer is negligible, outer surface temperature of the particle is uniform, and the surface temperature of the particle during cooling is changing. As the surface temperature changes, the convective heat transfer coefficient between the particle and the kerosene will also change. To avoid this, it is assumed that the surface temperature of the particle is constant at the average temperature (T_{avg}).

The Reynolds number of the flow is calculated as

$$Re = \frac{\varrho\, V\, D}{\mu_\infty} \tag{4.2}$$

where ϱ, V, μ_∞ are density, velocity and dynamic viscosity of kerosene and D is the diameter of steel particle. As the fluid flow is in μchannel the Reynolds number is less than 1.

The Prandlt number is calculated as

$$Pr = \frac{\mu_\infty\, Cp}{k} \tag{4.3}$$

where C_p and k are specific heat and thermal conductivity of kerosene.

According to Whitaker, Nusselt number for flow over spherical shape is given by [98]

$$Nu = \frac{h\, D}{k} = 2 + \left[\, 0.4\, Re^{1/2} + \, 0.06\, Re^{2/3} \,\right] Pr^{0.4} \left(\frac{\mu_\infty}{\mu_s}\right)^{1/4} \tag{4.4}$$

where h is the average heat transfer coefficient and $\frac{\mu_\infty}{\mu_s}$ is the ratio of dynamic viscosity. Time of cooling of the particle from 15000 K to 300 K is calculated by an average rate of heat transfer from Newton's law of cooling by using the average surface temperature. The average temperature (T_{avg}) is calculated as

$$T_{avg} = \frac{T + T_\infty}{2} \tag{4.5}$$

The surface area of a particle is calculated as

$$A_s = 4\pi r^2 \tag{4.6}$$

where r is the radius of particle

The average rate of heat transfer is calculated as [98]

$$\dot{Q}_{avg} = h \,.\, A_s \,.\, (T_{avg} - T_\infty) \tag{4.7}$$

Total heat transferred from the particle which is change in the energy of the particle as it cools from 15000 K to 300 K is calculated as

$$\dot{Q}_{total} = m \,.\, C_p \,.\, (T - T_\infty) \tag{4.8}$$

where m is the mass of the particle

Time of cooling of the particle is calculated as [98]

$$Time\ of\ cooling = \frac{\dot{Q}_{total}}{\dot{Q}_{avg}} \tag{4.9}$$

In this way, time of cooling of a particle of different size is calculated. The values of various parameters of particle and kerosene are listed in Table 4.5. and the time for cooling of particle is given in Table 4.6. The distance travelled by the particle before cooling is calculated by taking the product of time and velocity of the particle. The velocity of the particle is assumed equal to the velocity of the dielectric. The velocity values in the table shows the average dielectric velocity at different position in the IEG.

Table 4.5 Parameters of particles and kerosene

Parameters	**Values**		
Diameter, D (μm)	4	8	12
Surface area, A_s (μm^2)	50.26	201	452
Mass, m (gm)	2.6908×10^{-10}	2.152×10^{-9}	7.265×10^{-9}
Dynamic viscosity, μ (Kg/m s)	μ_s = 0.007 (steel), μ_∞ = 0.0024 (kerosene)		

Table 4.6 Cooling time of a particle at different positions in the IEG

Dia. (μm)	**Posi-tion**	**Re**	**Pr**	**Nu**	**h (W/m^2k)**	**Q_{avg} (J/s)**	**Q_{total} (J)**	**Time (ms)**	**Velo-city (cm/s)**	**Dist-ance (μm)**
Ø 4	**A**	0.022	33.66	2.20	81950	0.0303	1.99×10^{-6}	0.0657	1.68	1.10
	B	0.015		2.16	80535	0.0298		0.0668	1.12	0.75
	C	0.008		2.12	78933	0.0292		0.0682	0.62	0.42
Ø 8	**A**	0.044		2.28	42544	0.0629	1.59×10^{-5}	0.253	1.68	4.25
	B	0.029		2.23	41550	0.0614		0.259	1.12	2.90
	C	0.016		2.17	40427	0.0597		0.266	0.62	1.65
Ø 12	**A**	0.066		2.35	29180	0.0969	5.37×10^{-5}	0.554	1.68	9.3
	B	0.044		2.28	28363	0.0942		0.57	1.12	6.38
	C	0.024		2.21	27440	0.0912		0.589	0.62	3.65

4.6.2 Simulation Method

The simulation study is carried out by injecting particles of various diameter (4, 8, 12 μm) from the workpiece surface with a temperature of 15000 K. The particle is injected after 60 sec so that the maximum velocity of the dielectric is attained in the IEG. The particle is injected with a high velocity so that it will reach a desired position in the IEG (A, B, C). This is essential to study the cooling rate and the distance travelled by the particle when it is initially present at different position in the IEG. The time required by a particle to attain the temperature of dielectric (300 K) is given in Figure 4.13. When the particle of same size travels from different position in the IEG the time for cooling is nearly same.

However, with the increase in the size of the particle the time for cooling increases. The particle of size 4 µm cools rapidly as it comes in contact with the dielectric while the particle of 12 µm takes some time to cool. The reduction in temperature is very high when the particle in the first instance comes in contact with the dielectric, later the heat transfer rate reduces.

The temperature of the particle immediately after injection and its temperature after travelling some distance in the IEG is given in Figure 4.14 (a) and the trajectory followed is shown in Figure 4.14 (b). The initial and the final coordinates of the point is plotted in the AutoCAD software and the arc is drawn. The length of the arc represents the distance travelled and the trajectory of the particle. It is observed that if the particle is near the tool it covers longer distance irrespective to the size of the particle. And if the particle is near the workpiece it travels small distance and cools rapidly as the velocity of dielectric is less as shown in Figure 4.14 (c). The trajectory of the particle near the workpiece shows that the particle is dragged towards the center of the IEG due to higher velocity of dielectric in that region.

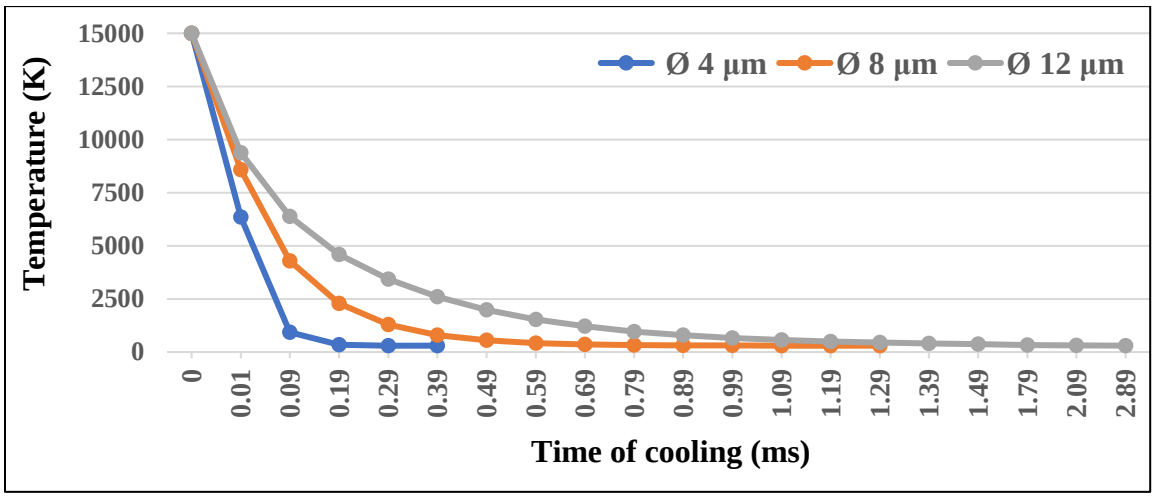

Figure 4.13 Time required for cooling of a particle initially at 15000 K to 300 K of various size

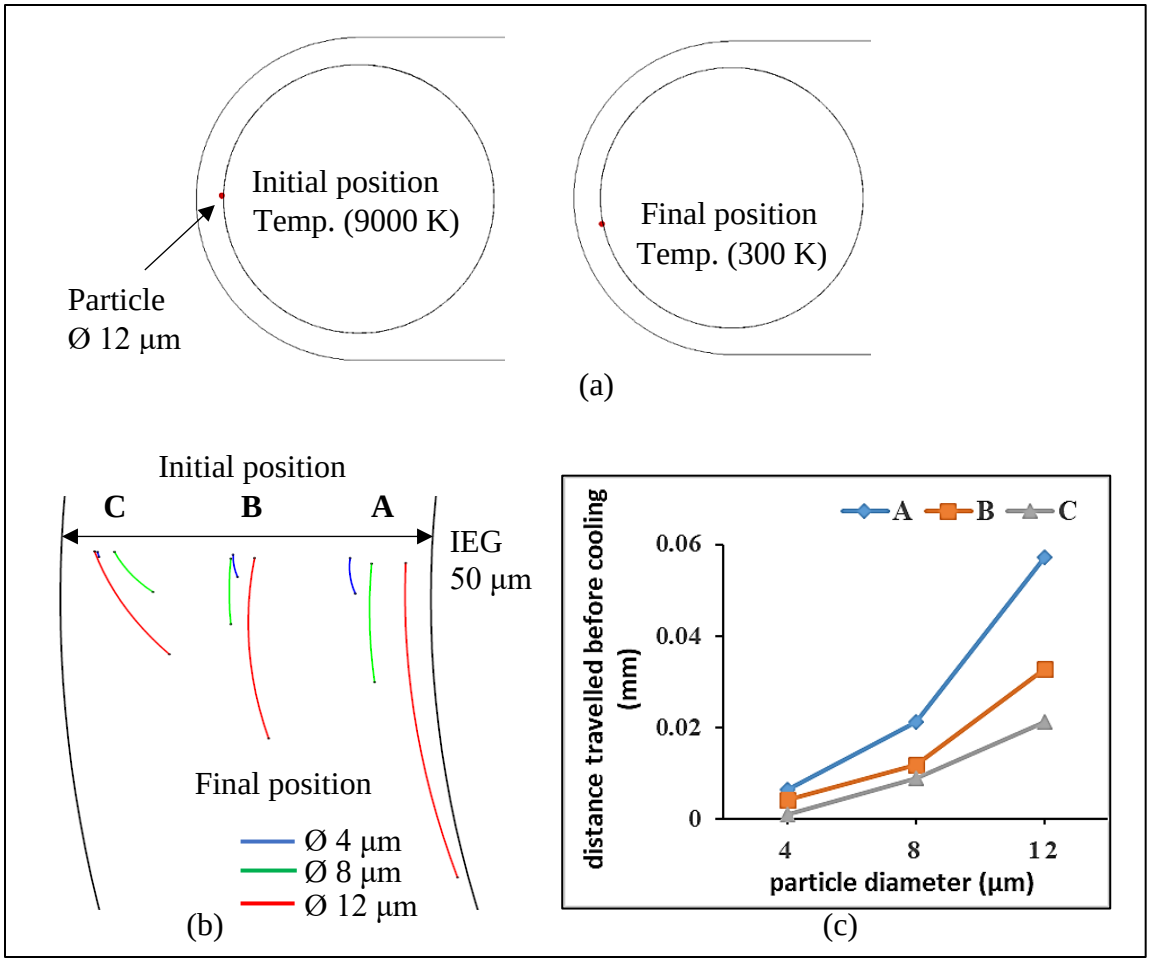

Figure 4.14 Plot showing (a) Particle temperature and its motion in the IEG (b) trajectory of the particles before cooling in the IEG, and (c) distance travelled

When the particle is not injected with a high velocity then it fails to move out of the workpiece surface. At the position of the injection, if the temperature of the workpiece surface is very high then the temperature of the dielectric surrounding it increases as shown in Figure 4.15. If the particle is present in this zone then it is heated to higher temperature. With the travel of the particle out of the zone its temperature decreases. This particle which is near to workpiece and is at sufficient temperature gets stick to nearby workpiece surface.

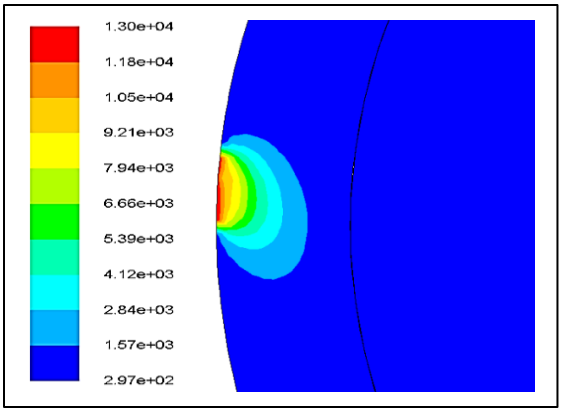

Figure 4.15 Temperature distribution in the IEG

The comparison between the analytical and simulation method is represented in Figure 4.16. It is seen from the figure that the analytical method showed less value of time as compared to simulation result. This is due to the assumption made in the analytical approach that the particle is stationary while in simulation it is moving. In addition to this, it will be imprecise to specify that the time for cooling the particle of particular size to be exactly the same by analytical approach. Taking this into consideration, it can be observed from the figure that the trend of the result obtained using analytical and simulation approach is similar. As the particle size is very small and it is at a very high temperature it cools within few milli-seconds due to large temperature difference.

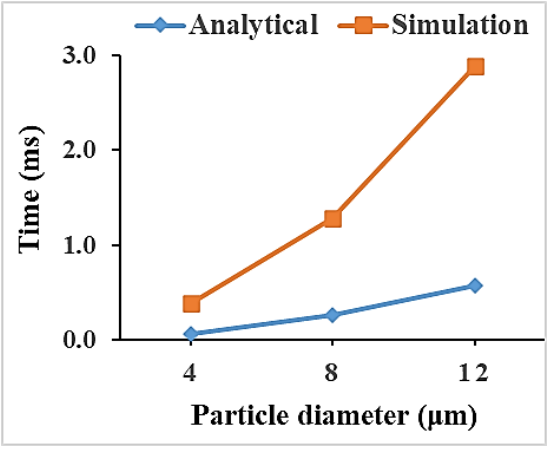

Figure 4.16 Comparison of the cooling time using analytical and simulation method

4.7. SUMMARY

The CFD simulation is very useful to study the trajectory of the debris in the gap. It is difficult to capture the debris movement in the gap using experimental method due to small gap of few microns. The major drawback of EDM process is that most of the material removed gets redeposited on the tool and the workpiece. So, it becomes necessary to study the trajectory of debris, to understand the redeposition phenomenon. The rotating dielectric fluid along the tool surface drags the debris from the sparking zone and gets redeposited on the workpiece. The debris combines together to form a cluster of particles, and also, chain-like structure is observed due to tool rotation. The accretion rate outside the sparking zone increases with the increase in the size of the particles. At higher tool speed, particles are flushed away from the gap without accreting on the workpiece. The debris gets deposited on one side of the μchannel due to centrifugal force exerted by the tool. The particle cools at a very high rate and the distance travelled mainly depends on the position of the particle in the IEG.